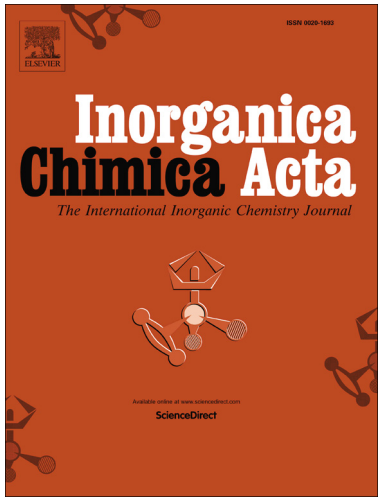

Research paper

Single Molecular Dual Analyte Thio-Urea based Probes for Colorimetric Hg^{2+} and Fluorometric AcO^- Detection and Its' Application in Bioimaging

Sumit Kumar Patra, Bhaskar Sen, Sanjoy Kumar Sheet, Bodhisattwa Banerjee, Nirmalendu Saha, Snehadrinarayan Khatua

PII: S0020-1693(18)31855-3
DOI: https://doi.org/10.1016/j.ica.2019.04.017
Reference: ICA 18862

To appear in: *Inorganica Chimica Acta*

Received Date: 14 December 2018
Revised Date: 20 March 2019
Accepted Date: 10 April 2019

Please cite this article as: S. Kumar Patra, B. Sen, S. Kumar Sheet, B. Banerjee, N. Saha, S. Khatua, Single Molecular Dual Analyte Thio-Urea based Probes for Colorimetric Hg^{2+} and Fluorometric AcO^- Detection and Its' Application in Bioimaging, *Inorganica Chimica Acta* (2019), doi: https://doi.org/10.1016/j.ica.2019.04.017

Single Molecular Dual Analyte Thio-Urea based Probes for Colorimetric Hg^{2+} and Fluorometric AcO^{-} Detection and Its'Application in Bioimaging

Sumit Kumar Patra,[a] Bhaskar Sen,[a] Sanjoy Kumar Sheet,[a] Bodhisattwa Banerjee,[b] Nirmalendu Saha,[b] Snehadrinarayan Khatua* [a]

[a]*Centre for Advanced Studies, Department of Chemistry, North Eastern Hill University, Shillong, Meghalaya 793022, India. Email: snehadri@gmail.com; skhatua@nehu.ac.in*

[b]*Department of Zoology, North Eastern Hill University, Shillong, Meghalaya 793022, India.*

Abstract

Two thio-urea based bifunctional probes (**H_2L^1-S** and **H_2L^2-S**) have been designed and fabricated for the colorimetric and fluorometric detection of mercury(II) and acetate ions respectively in DMSO media. Both the **H_2L^1-S** and **H_2L^2-S** were fully characterized by various spectroscopic techniques and the solid-state structure of **H_2L^1-S** was determined via single-crystal X-ray diffraction. The high sensitivity and selectivity of the probes for Hg^{2+} were achieved by the Hg^{2+} promoted desulfurization reactions utilizing the high thiophilic nature of mercury and was monitored by UV–vis spectroscopy. Most interestingly the desulfurized product was isolated and characterized by ESI-MS and single crystal X-ray diffraction. The probes **H_2L^1-S** and **H_2L^2-S** were found to be highly selective towards acetate ion (AcO^-) in fluorescence channel. These probes showed a distinct fluorescence enhancement only in the presence of AcO^- at 493 nm due to the inhibition of photo induced electron transfer (PET). Finally, the cytotoxicity study was carried out for biological application. The probe showed minimum cytotoxicity and was suitable for intracellular acetate ion imaging.

Keywords: Thio Urea; Bifunctional probe; Hg^{2+} detection; AcO^- detection, Bioimaging

1. Introduction

The development of single molecular multifunctional probe is an expanding area of chemistry because of their wide practical application in the environmental and medical fields [1-3]. Several strategies were already employed for multianalyte probes: (I) incorporation of several binding sites, one for each analyte [4-6], (II) operating in single channel at different experimental condition [7-9] and (III) single receptor in different channel interrogation, ideally one channel per analyte [10-12]. In contrast to approaches (I) and (II), detection through different channel interrogation which differently react with probe is more facile and advantageous from a synthetic and atom-economic point of view. To date, there have been several reports on single molecular bifunctional probes for multi cations [13-15] and multi anions [16-18], but highly selective and sensitive detection for both cation and anion in two different channels with different mode of action are rarely reported [19-20].

Among variety of heavy metal ions, mercury(II) ion (Hg^{2+}) is one of the most toxic metal ions which widely distributed in water and soil, especially those originated from chemical industries [21-23]. Hg^{2+} metabolism by aquatic microbes produces methyl mercury, which is a highly potent neurotoxin that leads to many serious human afflictions, such as Minamata, edema and anemia, damage the central nervous system, even a very low concentration [24-26]. Therefore, rapid and competent detection of Hg^{2+} has become very vital to control its concentration level in environmental and biological samples to avoid its direct impact in human health [27-29]. Recently, colorimetric methods for detection of Hg^{2+} are becoming a potential contender for replacing the traditional instrument-based methods due to its operational simplicity, high selectivity, sensitivity, rapidity, low cost of equipment and direct visual perception [30-32].

The recognition and sensing of various inorganic and biotic anions such as acetate, phosphate, and halide, has attracted significant interest for their fundamental role in a wide

range of chemical and biological Processes [33-34]. In particular, the acetate anion has long been perceived as a crucial cellular molecule involved in several metabolic processes. The rate of acetate production and oxidation has been usually used as an indicator of organic decomposition in aquatic sediments and transmetalation of tetrapyrroles [35-36]. Industrially, acetate ion is very much important not only as a raw material in the nylon industry but also for their use in manufacturing paper, cosmetics, plastics, dyes and paints [37]. Currently, many elegant techniques are available for qualitative and quantitative analysis of acetate ions, however, these methods are less satisfactory for endogenous detection of acetate ion due to tedious sample preparation procedures, sophisticated instruments and high maintenance expenditure [38-39]. To realize in situ visualization of AcO^- within a living cell, there is a growing interest to develop small molecule based fluorescent probes in view of their high sensitivity, good selectivity and real-time detection [40-42].

Among the variety of signal transductions, photo induced electron transfer (PET) has been successfully employed in fluorescent sensor design for different analytes by many groups [43-44]. Upon excitation of the fluorophore, PET occurs from electron rich group to electron deficient module. The interaction of analytes with electron donating or electron withdrawing group are preventing the PET by obstructed the electron transfer process resulting switch-ON of the fluorescence [45].

For several decades thio-urea based receptors have been acclaimed for detection of either F^- and AcO^- or Hg^{2+} ion [46-47]. As part of our ongoing research in small organic, ruthenium(II) and organoiridium(III)-complex based multifunctional probes [48-52], herein we present the synthesis of two simple thio-urea based bifunctional probes (**H_2L^1-S**, **H_2L^2-S**) and their aptness for highly sensitive and selective detection of Hg^{2+} and AcO^- ions by two distinct detection approaches. These probes selectively detect Hg^{2+} in the UV−vis spectroscopy through the colour change from yellow to colourless associated with a notable

blue shift. The very weakly emissive probes **H_2L^1-S** and **H_2L^2-S** selectively interact with AcO^- rapidly (within 1.5 mins) and emits strongly at 493 nm. Finally, the cytotoxicity and the intracellular AcO^- imaging in live cell are also discussed herein. To the best of our knowledge there is no such report on a single molecular thio-urea based probe for detection of two analytes, namely toxic Hg^{2+} and biologically important AcO^- in two different spectroscopic channels through different reaction mechanism.

2. Experimental

2.1. Material and physical measurements

All chemicals were used as received from commercial suppliers (Aldrich, Alfa Aesar and Spectrochem India). ^1H and ^{13}C NMR spectra were measured on a Bruker Avance II (400MHz) spectrometer and chemical shifts were expressed in ppm using using residual protic solvent as the internal standard . ESI-MS was performed with a Waters ZQ-4000 and QToF−Micro YA 263 mass spectrometer. Infrared spectra were recorded using a Perkin-Elmer FT- IR spectrometer with KBr pellets in the range of 4000–400 cm^{-1}. The X-ray data was collected at 293 K with a Agilent Xcalibur (Eos, Gemini) diffractometer and Bruker KAPPA APEX II CCD diffractometer using graphite-monochromated Mo-*K*α radiation (λ = 0.71073 Å). Elemental analysis were done using the PerkinElmer 2500 series II elemental analyzer. UV-visible and PL spectra were recorded on a Perkin-Elmer Lambda 25 UV–vis spectrophotometer and Hitachi F-4500 fluorescence spectrophotometer with quartz cuvette (path length = 1 cm).

2.2. Methodology for UV-vis experiments

In the UV-vis channel, the measurements were conducted as follows. Firstly, the stock solutions of **H_2L^1-S** and **H_2L^2-S** were prepared at a concentration of 100 μM in DMSO. All perchlorate salt of cation including $Hg(ClO_4)_2$ were used to prepare the stock solution in water (10 mM). Before the measurements, the probe stock solution of **H_2L^1-S** and **H_2L^2-S**

were diluted to 20 μM, and then the Hg^{2+} was added into the diluted probe solution and UV–vis spectra were recorded at room temperature immediately. All spectra of H_2L^1-S and H_2L^2-S were recorded in 30% and 5% aqueous DMSO solution respectively.

2.3. Methodology for emission experiments

A stock solution (1 mM) of the probe **H_2L^1-S** and **H_2L^2-S** were prepared in DMSO which were diluted to 20 μM or 50 μM before data collection. DMSO solution of all anions including tetra-*n*-butyl ammonium acetate (100 mM) were prepared. Samples for emission measurement were contained in 1 cm × 1 cm quartz cuvettes (3.5 mL volume). All spectroscopic measurements of **H_2L^1-S** and **H_2L^2-S** were performed in DMSO solution. An excitation wavelength at 412 nm and 405 nm was used for probe **H_2L^1-S** and **H_2L^2-S** respectively. Excitation and the emission slit were set to 10 mm/10 nm and the PMT voltage at 700 V.

2.4. Calculation of excited states lifetimes

The luminescence lifetime of **H_2L^1-S** and **H_2L^2-S** before and after addition of AcO^- were carried out under ambient conditions using a time-correlated single-photon counting (TCSPC) spectrometer [a picosecond diode laser (IBH, UK)] with the detection wavelength at 493 nm for **H_2L^1-S** and **H_2L^2-S** both in the presence and absence of AcO^- (λ_{ex} = 412 nm and 405 nm for **H_2L^1-S** and **H_2L^2-S** respectively). The fluorescence decays were monitored at the corresponding emission maxima as observed in the steady state fluorescence measurement. The fluorescence decay data were collected on a Hamamatsu MCP PMT (R3809) and were analysed by using IBH DAS 6 software. Nano LED at 416 nm was used as the excitation source. All the fluorescence decays were fitted with a biexponential function considering a χ^2 value close to 1, which is an indication of good fitting. Experimental time-resolved luminescence data were calculated using the following multiexponential decay equation

$$<\tau> = \sum a_i \tau_i$$

Whereas, a_i is the amplitude of the i^{th} decay component ($a_i = \alpha_i/\Sigma\alpha i$) and τ_i is the excited state luminescence life time of the i^{th} component.

2.5. Determination of detection limit

The detection limit (DL) of the probes **H_2L^1-S** and **H_2L^2-S** was calculated based on the fluorescence titration data and according to the equation DL = 3 × SD/slope, Where SD is the standard deviation of the blank solution (obtained by the 10 consecutive scan of the blank sample)

2.6. Quantum Yield Calculation

The fluorescence quantum yield was determined using fluorescein (Φ_R = 0.91 in 0.1 M NaOH) as an optically matching standard. The quantum yield is calculated according to the following equation:

$$\phi_x = \phi_s (F_x/F_s) \{(1\text{-}10\text{^-}A_s)/ 1\text{-}10\text{^-}A_x)\} (\eta_x/\eta_s)^2$$

Here, Φ_X and Φ_S are the fluorescence quantum yield of the probe and standard respectively. F_X and F_S are the integrated area under the corrected emission spectra of the probe and the standard, respectively. A_x and A_S are the corresponding absorbance of probe and standard at the excitation wavelength and η is the refractive index of the solvents.

2.7. Synthesis of 1-(4-methylbenzo[d]thiazol-2-yl)-3-(4-nitrophenyl) thiourea (H_2L^1-S)

The synthetic route of 1-(4-methylbenzo[d]thiazol-2-yl)-3-(4-nitrophenyl) thiourea (**H_2L^1-S)** is depicted in **Scheme 1**. 2-amino-4-methylbenzothiazole (0.33 g, 2.00 mmol) and 4-nitrophenyl isothiocyanate (0.40 g, 2.20 mmol) were dissolved in 15 ml of dry CH_3CN. Then the mixture was refluxed for 3 hours under N_2. An off-white precipitate was obtained after 30 mins and the reaction was continued for 3 hours. The precipitate was collected by filtration and washed thoroughly with CH_3CN and diethyl ether and then dried under vacuum. Yield:

50% (0.320 g). M.P = 228-233 °C. Elemental analysis: calcd. (%) for $C_{15}H_{12}N_4O_2S_2$ (MW = 344.41): C, 52.31; H, 3.51; N, 16.27; found: C, 52.35; H, 3.49; N, 16.28; FTIR in KBr disk (ν_{max} /cm^{-1}): 2956, 1575, 1515, 1335, 1264, 1193, 849, 740, 693. ESI-MS (positive mode): (*m/z*, %): 345.05 [$(C_{15}H_{12}N_4O_2S_2+H)^+$, 100%]; calcd. *m/z*, 345.04]; ^{1}H-NMR (400 MHz, DMSO-d_6): δ (ppm) = 13.21 (s, 1H, H_a), 10.94 (s, 1H, H_b), 8.21 (d, *J* = 8.8 Hz, 2H, H_2, $H_{2'}$), 8.14 (d, *J* = 8.8 Hz, 2H, H_3, $H_{3'}$), 7.73 (d, *J* = 7.2 Hz, 1H, H_9), 7.23- 7.30 (m, 2H, H_{10},H_{11}), 2.57 (S, 3H, H_{12}); ^{13}C-NMR (100 MHz, DMSO-d_6): δ (ppm) = 145.8 (2C,C_1, C_5), 141.8 (1C, C_4), 128.1 (3C, C_7, C_{10}, C_{12}), 124.6 (2C, C_2, $C_{2'}$), 124.0 (1C, C_{11}), 120.8 (2C, C_3, $C_{3'}$), 120.1 (3C, C_6, C_8, C_9), 17.9 (1C, C_{13}).

2.8. Synthesis of 1-(1H-benzo[d]imidazol-2-yl)-3-(4-nitrophenyl) thiourea (H_2L^2-S)

Synthesis of 2-(4-naphthalen-1-yl-phenyl)-2H-[1,2,3] triazole-4-carbaldehyde (**H_2L^2-S**) is shown in **Scheme 1**. A mixture of 2-amino benzimidazole (0.27 g, 2.00 mmol) and 4-nitrophenyl isothiocyanate (0.40 g, 2.20 mmol) was refluxed in dry CH_3CN under N_2 for 3 hours. A greenish yellow precipitate was appeared after 30 mins and the reaction was continued to 3 hours to complete the conversion. The precipitate was collected by filtration, washed with CH_3CN and diethyl ether thoroughly and dried under vacuum. Yield: 61% (0.382 g). M.P = 217-222 °C. Elemental analysis: calcd. (%) for $C_{14}H_{11}N_5O_2S$ (*MW* = 313.33): C 53.66, H 3.54, N 22.35; found: C 53.70, H 3.52, N 22.38; FTIR in KBr disk (ν_{max} /cm^{-1}): 3259, 1621, 1582, 1547, 1453, 1323, 1295, 1246, 1112, 848, 747. ESI-MS; (positive mode): (*m/z*, %): 314.07 [$(C_{14}H_{11}N_5O_2S + H)^+$, 100%]; calcd. m/z, 314.06; ^{1}H-NMR (400 MHz, DMSO-d_6): δ (ppm) = 12. 95 (s, 2H, H_a, H_b), 10.39 (s, 1H, H_c), 8.11-8.16 (m, 4H, H_2, $H_{2'}$, H_3, $H_{3'}$), 7.52-7.55 (m, 2H, H_{10}, H_{12}), 7.24-7.27 (m, 2H, H_9, H_{11});^{13}C-NMR (100 MHz, DMSO-d_6): δ (ppm) = 153.0, 146.6, 140.9, 128.9, 124.5, 123.1, 121.1, 119.9, 111.9, 111.4.

2.9. Cytotoxicity Study.

The cytotoxicity of the probe **H_2L^1-S** on HEK293T cells was determined by MTT assay as described by Mosmann, (1983) in a 96-well cell culture plate. The cells were seeded in a 96-well plate containing 2 ml of DMEM (Dulbecco's Modified Eagle Medium) at a density of 4 × 10^3 cells/well and incubated at 37 °C, 5% CO_2 incubator. Cells were treated with at different concentration (5, 10, 25, 50, and 100 μM) at 70% confluency and incubated for 24 h. After incubation, media was replaced by same volume of serum free DMEM media and MTT salt was added in medium to a final concentration of 0.5 mg/ml. The plate was incubated for 4 hours at 37 °C until intracellular purple formazan crystals were visible under microscope. After incubation, the media was discarded and 200 μl of DMSO was added in well. The DMSO was mixed with purple formazan salt by shaking the plate gently. The absorbance change was monitored at 570 nm using iMark™ (Bio-Rad, USA) microplate absorbance reader. Readings were taken in triplicate and the % cell viability was calculated for samples and controls based on the following formula:

$$\% \text{ cell viability} = \{(Abs_{treated} - Abs_{blank}) / (\text{Abs of control} - \text{Abs of blank})\} \times 100$$

2.10. Cell Culture and Imaging.

Cells were seeded at normal confluency (~10%) in 12 well sterile culture plates on poly-l-lysine coated coverslips containing 2 ml of DMEM (Dulbecco's Modified Eagle Medium) medium and incubated inside a CO_2 incubator at 37 °C with 5% CO_2 supplemented with 1% streptomycin penicillin and 10% FBS (Fetal Bovine Serum). When the cells were approximately 70% confluent, fresh media was added in two successive wells. One well was treated with 50 μM aqueous solution of **H_2L^1-S** (20% DMSO as co solvent) and incubated for 30 min. Afterward, 50 μM of AcO^- was added and incubated for 10 min. The other well was treated with only **H_2L^1-S** (50 μM) and incubated for 30 min. After incubation, cells were washed with 500 μl of HBSS (Hank's Balanced Salt Solution) and fixed with chilled absolute ethanol. Further, the cells were washed three times with HBSS (500 μl) to remove residual

ethanol. After washing, the cell containing coverslips were mounted on glass slides. Another set of slides were processed in the same way except incubation with probes, which served as negative controls. Imaging studies of probe **H_2L^1-S** were performed by conducting fixed-cells imaging experiments by confocal laser scanning microscope (Leica, TCS SP5, Germany). Cross-talk of fluorochromes was excluded by the use of the acousto optical tunable filter.

2.11. Theoretical study

The electronic properties of all probes and their final products were investigated by means of density functional theory (DFT) calculations [53]. All calculations were performed using the B3LYP exchange correlation functional, as implemented in the Gaussian 03(G03) program package [54]. The 6–31G (d, p) basis set was assigned for all the elements.

2.12. Crystallographic studies

The X-ray data of **H_2L^1-S and H_2L^1-O** was collected at 293 K with Agilent Xcalibur (Eos, Gemini) diffractometer and Bruker KAPPA APEX II CCD diffractometer using graphite-monochromated Mo-*K*α radiation (λ = 0.71073 Å). For **H_2L^1-S** the data was collected and reduced in CrysAlis PRO software [55]. The absorption was corrected by SCALE3 ABSPACK multi-scan method in CrysAlisPro. The structures were solved by direct methods using the program SHELXS-97 [56] and refined by full matrix least-squares calculations (F^2) by using the SHELXL-2014 [57] software. For **H_2L^1-O** the data integration and reduction were processed with SAINT [58] software. A multi-scan absorption correction (SADABS) [59] was applied to the collected reflections. The structures were solved by direct methods using the program SIR92 [60] and refined by full matrix least-squares calculations (F^2) by using the SHELXL-2014 [57] software. For both compounds all non-H atoms were refined anisotropically against F^2 for all reflections. All hydrogen atoms except N-H were placed at their calculated positions and refined isotropically. The N-H hydrogen was found on a difference Fourier map and refined isotropically. Structure analysis was aided by use of the

programs PLATON [61]. The cif files were deposited with the Cambridge Crystallographic Data Centre and the following codes were allocated for **(H_2L^1-S)** and **(H_2L^1-O)** respectively: CCDC-1539236 and CCDC-1539237. This data can be obtained free of charge *via* the Internet: www.ccdc.cam.ac.uk/ data request/cif. Crystal data collection and refinement details, for probe **(H_2L^1-S)** and **(H_2L^1-O)** are given in Table 1 and selected bond lengths and angles are given Table S2 and Table S3.

Table 1. Crystal data and structure refinement for **H_2L^1-S** and **H_2L^1-O**

	H_2L^1-S	**H_2L^1-O**
Empirical formula	$C_{17}H_{18}N_4O_3S_3$	$C_{17}H_{18}N_4O_4S_2$
Formula weight	422.53	406.47
Temperature	293(2) K	293(2) K
Wavelength	0.71073 Å	0.71073 Å
Crystal system	Monoclinic	Monoclinic
Space group	$P2_1/c$	$P2_1/c$
Unit cell dimensions	a = 10.1731(8) Å	a = 9.9940(11) Å
	b = 22.6224(19) Å	b = 9.8485(10) Å
	c = 8.6431(5) Å	c = 19.010(2) Å
	α = 90°	α = 90°
	β = 99.600(6) °	β = 96.451(4) °
	γ = 90°	γ = 90°
Volume, Z	1961.3(3) $Å^3$,4	1859.3(4) $Å^3$, 4
Density (calcd.)	1.431 Mg/m^3	1.452 Mg/m^3
Absorption coefficient	0.404 mm^{-1}	0.318 mm^{-1}
F (000)	880	848
Θ range for data collection	3.38 to 26.37°.	2.804 to 25.071°.
Reflections collected	7598	32484
Independent reflections	3999 [R(*int*) = 0.0260]	3296 [R(*int*) = 0.0814]
Refinement method	Full-matrix least-squares on F^2	Full-matrix least-squares on F^2
Data / restraints / parameters	3999 / 0 / 255	3296 / 0 / 255
Goodness-of-fit on F^2	1.028	1.085
Final *R* indices [$I>2\sigma(I)$]	*R*1 = 0.0525, *wR*2 = 0.1027	*R1* = 0.0489, *wR2* = 0.1097
R indices (all data)	*R*1= 0.0800, *wR*2 = 0.1141	*R1* = 0.0647, *wR2* = 0.1178

3. Result and Discussion

3.1 *Synthesis and characterization*

The benzothiazole and benzimidazole attached thiourea based probes **H_2L^1-S** and **H_2L^2-S** were synthesized by refluxing 4-nitrophenyl isothiocyanate with 2-amino-4-methylbenzothiazole and 2-aminobenzoimidazole in CH_3CN under N_2 atmosphere for 3 hours respectively (Scheme 1). The probes, **H_2L^1-S** and **H_2L^2-S** were fully characterized by elemental analysis, 1D (^1H, ^{13}C) and 2D NMR spectroscopy, ESI-MS spectrometry (Figure S1- S12). The solid-state structure of **H_2L^1-S** was determined by the single crystal X-ray diffraction (Figure 1). Photophysical properties were determined by UV−vis and PL spectroscopy. NMR spectra of **H_2L^1-S** and **H_2L^2-S** were recorded in DMSO-d_6 at room temperature, clearly showed all expected resonance. All the proton and carbon signals of **H_2L^1-S** and **H_2L^2-S** are fully assigned with the help of ^1H-^1H COSY, ^1H-^{13}C HSQC and ^1H-^{13}C HMBC NMR spectra. The ESI-MS spectra of **H_2L^1-S** and **H_2L^2-S** exhibited peaks at *m/z* =345.05 (calcd. 345.04) and 314.07 (calcd. 314.06) respectively, which are assigned to singly positive charged species.

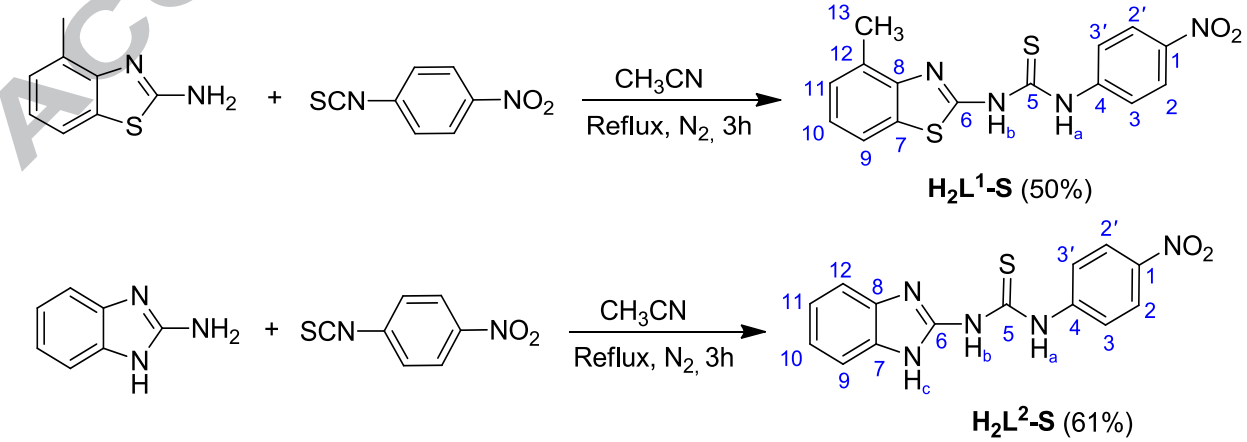

Scheme 1. Synthesis of probe, **H_2L^1-S** and **H_2L^2-S.**

3.2 Crystal structure description of compound H_2L^1-S.

The diffraction quality yellow, plate like single crystals of the compound **H_2L^1-S** was obtained from diethyl ether diffusion in DMSO after two weeks. The compound was crystallized in monoclinic space group $P2_1/c$. The asymmetric unit contains the compound **H_2L^1-S** and a DMSO molecule as a solvent of crystallization (Figure 1a). Analysis of the crystal packing in **H_2L^1-S** reveals that the compound forms noncovalent 2D zig-zag sheet (Figure 1b and 1c) which is held together by weak C−H···O, N−H···O and C−H···S hydrogen bonding interactions. The oxygen centres (O1 and O2) of nitro group form H-bond with C(4)-H of benzothiazole and C(17)-H of solvent DMSO molecule respectively. Further, the S2 and N(2)-H of thio urea form hydrogen bond with C(5)-H of neighbouring probe molecule and O3 of solvent DMSO. The packing structures indicate that the solvent DMSO molecule plays an important role in formation of the zig-zag 2D sheet.

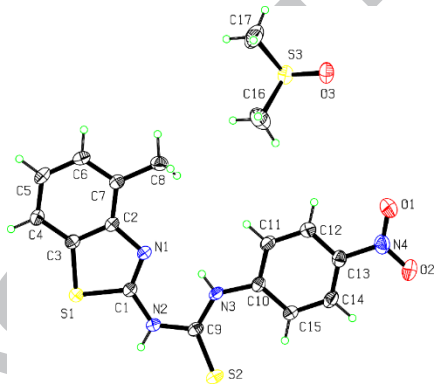

(a)

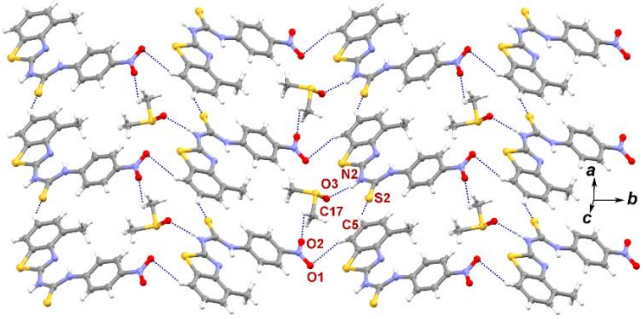

(b)

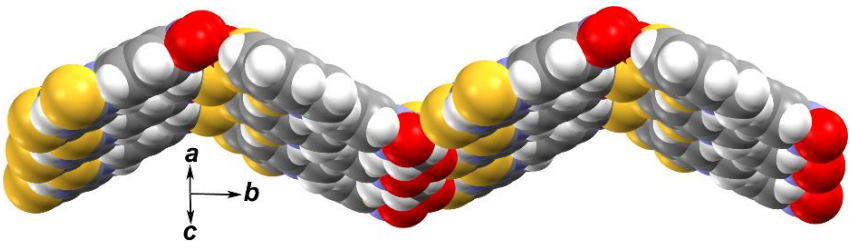

(c)

Figure 1. (a) ORTEP diagram of **H_2L^1-S** with 30 % ellipsoid probability. (b) View of the hydrogen bonded 2D *zig-zag* sheet along crystallographic *c*-axis. (c) Space filling model of the *zig-zag* sheet.

3.3 *Detection of Hg^{2+} in UV-vis spectroscopy*

3.3.1 Selectivity and Sensitivity of H_2L^1-S and H_2L^2-S to Hg^{2+}

Both the probes, **H_2L^1-S** and **H_2L^2-S** were used for the detection of various cations like Na^+, K^+, Mg^{2+}, Ca^{2+}, Fe^{2+}, Co^{2+}, Ni^{2+}, Zn^{2+}, Ag^+, Cd^{2+}, Pb^{2+}, Al^{3+} and Hg^{2+} by UV−vis spectroscopy in aqueous DMSO solution. For **H_2L^1-S** all data was collected in 30% aqueous DMSO solution, since, up to 30% aqueous DMSO solution notable change in UV-Vis spectrum and by naked eye was clearly observed in presence of only 1 equiv. of Hg^{2+}(Figure S13). Whereas, in the case of **H_2L^2-S,**with increase in the water fraction above 5% no notable colour change was observed in the presence of Hg^{2+}. Upon the addition of various cations to the 30% aqueous DMSO solution of **H_2L^1-S** (20 μM), the n-π^* band at 370 nm (ε = 25200 $Lmol^{-1}cm^{-1}$) was blue-shifted to 340 nm (ε = 21750 $Lmol^{-1}cm^{-1}$) and a prominent colour change from yellow to colourless can be readily observed by the naked eye only in the presence of Hg^{2+} (Figure 2a). Likewise, **H_2L^2-S** (20 μM) in the presence of Hg^{2+} shows a distinguished colour change from yellow to colourless and a notable blue shift (~8 nm) in 5 % aqueous DMSO solution (Figure 2b). In contrast, no significant shift of λ_{max} and the color were observed in the presence of other cations. The addition of increasing amounts of Hg^{2+} (0-1.0 equiv.) to **H_2L^1-S** (20 μM) in 30% aqueous DMSO solution at room temperature reveals a gradual blue shift of the absorption band from 370 nm to 340 nm (Figure 3a). Whereas, during the UV-vis titration of **H_2L^2-S** (20 μM) with increasing amount of Hg^{2+} (0-25 equiv.), a gradual blue shift of the absorption band from 375 (ε = 23000 $Lmol^{-1}cm^{-1}$) to

367 nm (ε = 18150 $Lmol^{-1}cm^{-1}$) is observed (Figure 3b). In addition, a new band is appeared slowly at 270 nm (ε = 34750 $Lmol^{-1}cm^{-1}$).

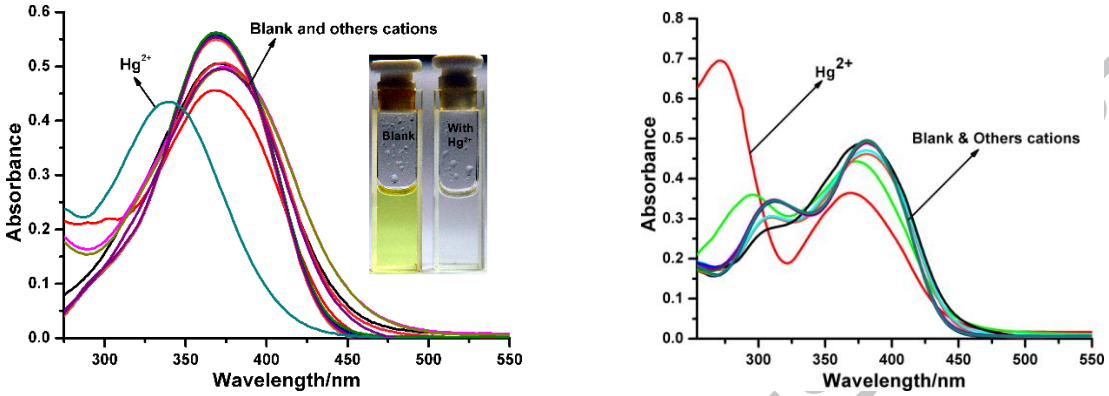

(a) (b)

Figure 2. UV-vis spectra of (a) **H_2L^1-S** (b) **H_2L^2-S** (20 μM) upon addition of various metal ions (Hg^{2+}, Al^{3+}, Na^+, K^+, Mg^{2+}, Ca^{2+}, Mn^{2+}, Co^{2+}, Ni^{2+}, Cu^{2+}, Zn^{2+}, Pb^{2+}, Ag^+, and Cd^{2+},) in 30% and 5% aqueous DMSO solution. (Inset) Naked eye visible color change of in addition of Hg^{2+} in **H_2L^1-S**.

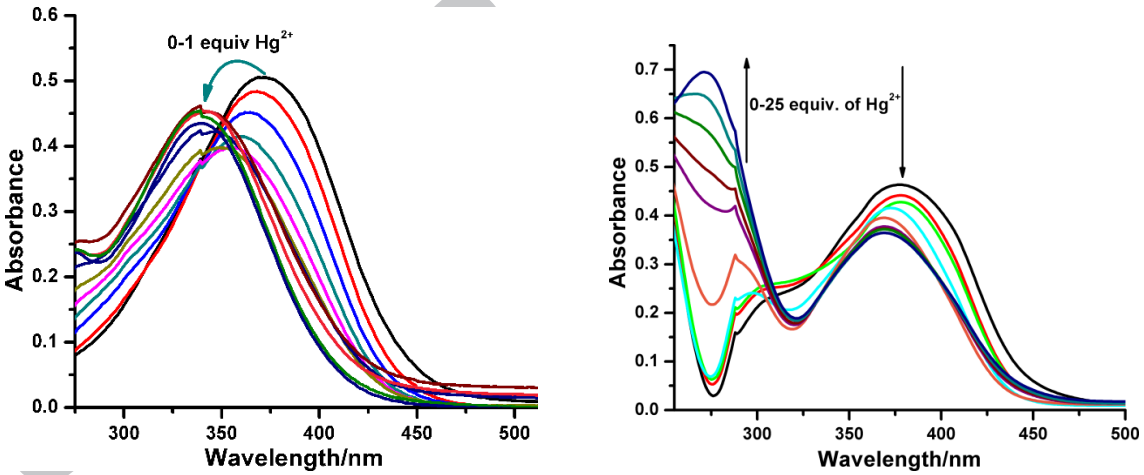

(a) (b)

Figure 3. UV−vis titration of (a) **H_2L^1-S** (20 μM) (b) **H_2L^2-S** (20 μM) with increasing amount of Hg^{2+} solution (0-1 equiv. and 0-25 equiv.) in 30% and 5% aqueous DMSO solution respectively.

A competition experiments with other metal ions were carried out in UV-vis spectroscopy to check for possible interferences in Hg^{2+} detection. Addition of other metal ions in excess (5.0 equiv.) did not influence the UV-vis response of probe **H_2L^1-S** (Figure 4a)

and **H_2L^2-S** (Figure 4b) for Hg^{2+}detection, indicating the high selectivity and sensitivity towards Hg^{2+}.

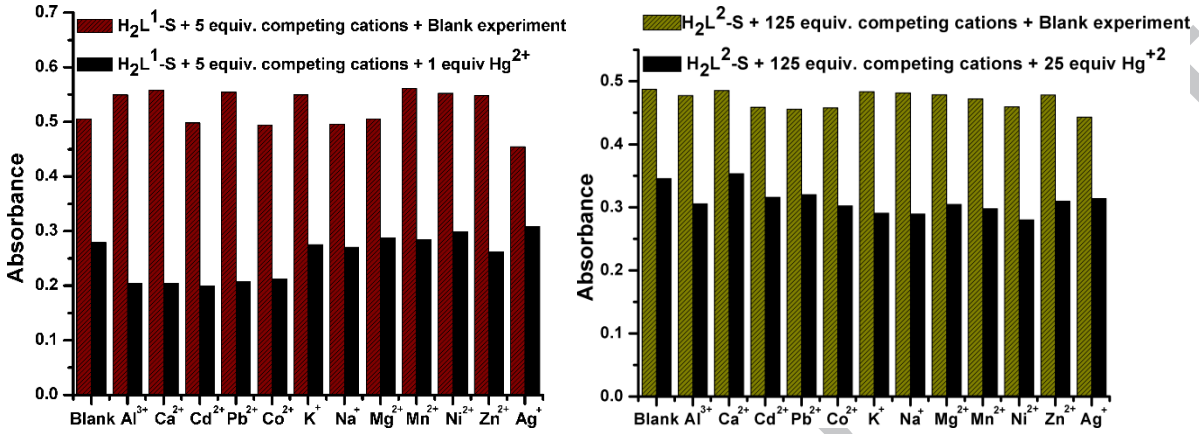

(a) (b)

Figure 4. The UV response of (a) **H_2L^1-S** (20 μM) (b) **H_2L^2-S** (20 μM) in the presence of various competing cations (5 equiv. and 125 equiv.) without and with Hg^{2+} (1 equiv. and 25 equiv.) in 30% and 5 % aqueous DMSO solution at 370 nm and 375 nm respectively.

The time course for the Hg^{2+} detection by **H_2L^1-S** and **H_2L^2-S** in 30% and 5 % aqueous DMSO solution at room temperature was monitored. An immediate absorbance and respective colour change was observed for **H_2L^1-S** (<40 s) (Figure 5a), while for **H_2L^2-S** ~2.5 mins after Hg^{2+} addition was essential for complete reaction (Figure 5b).

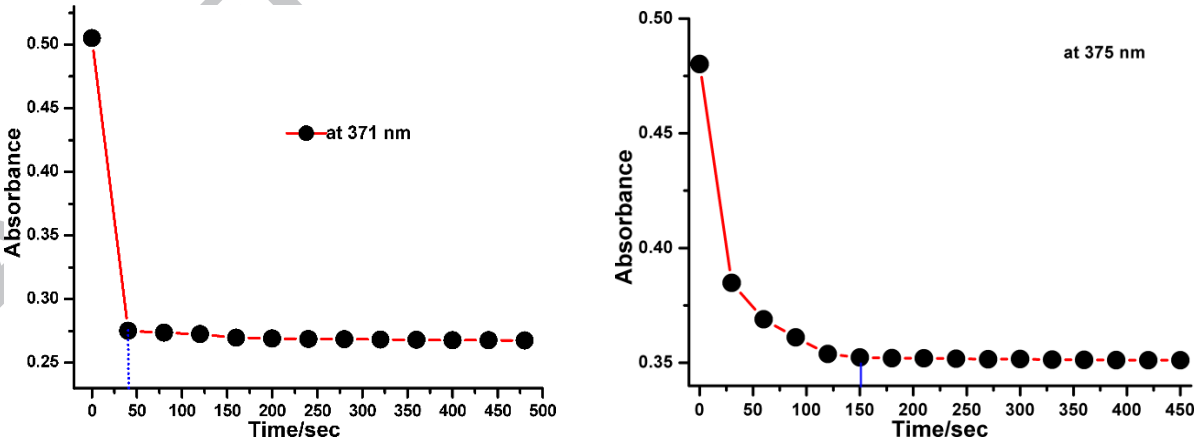

(a) (b)

Figure 5. Time course of the UV response of (a) **H_2L^1-S** and (b) **H_2L^2-S** upon addition of 1 equiv. and 25 equiv. of Hg^{2+} at 370 and 375 nm respectively.

3.3.2 The plausible mechanism of Hg^{2+} detection and supporting evidences

Similar to reported S-based Hg^{2+}probes [62], herein, we assume that the Hg^{2+} selective signalling by **H_2L^1-S** and **H_2L^2-S** is due to the Hg^{2+}-promoted desulfurization of thiourea derivative (Scheme 2). According to previous reports [62], due to the interaction of Hg^{2+} (soft acid) with sulphur center (soft base) of thiourea, the thio urea carbon (C=S) in **H_2L^1-S** and **H_2L^2-S** will be more electrophilic and attacked by water more easily, leading to the formation of 1-(4-methylbenzo[d]thiazol-2-yl)-3-(4-nitrophenyl) urea (**H_2L^1-O**) and 1-(1H-benzo[d]imidazol-2-yl)-3-(4-nitrophenyl) urea (**H_2L^2-O**). In **H_2L^1-S**, the Hg^{2+} assisted desulfurization reaction is more facile because of the presence of two 'S' atoms which assist the chelation with Hg^{2+}. Consequently, only 1 equiv. of Hg^{2+} is required for desulfurization of **H_2L^1-S** and the reaction completed within 40 seconds. Whereas, in **H_2L^2-S,** the desulfurization reaction is comparatively slow (2.5 minute) and require ~25 equiv. of Hg^{2+} since the probe contain only one 'S' atom and the coordination with Hg^{2+} is weaker.

To verify the mode of interaction, we performed a reaction of **H_2L^1-S** and **H_2L^2-S** with $HgClO_4{\cdot}6H_2O$ in 5 % aqueous DMSO solution and characterized the reaction mixture by ESI-MS. In ESI-MS spectra, a peak at m/z = 345.05 (calcd. m/z = 345.04) for compound **H_2L^1-S** entirely vanished with a generation of new peak at m/z = 329.06 attributed to desulfurized product, **H_2L^1-O** (calcd. m/z =329.06) (Figure S14). Similarly, for **H_2L^2-S** a new peak at 298.08 (calcd. m/z = 298.09), corresponding to $[C_{14}H_{11}N_5O_3 + H]^+$ confirm the formation of desulfurized product **H_2L^2-O** (Figure S15). Finally, the isolated desulfurized product, **H_2L^1-O** was structurally characterized by single crystal X-ray diffraction. (Figure 6). The diffraction quality crystal was obtained from ether diffusion in DMSO solution. The **H_2L^1-O** was crystallized in monoclinic $P2_1/c$ space group. The asymmetric unit contains the compound **H_2L^1-O** and a DMSO molecule as a solvent of crystallization. In the compound, the solvent DMSO molecule forms H-bond with the N-H hydrogens of the urea (Figure 6b).

The crystal packing analysis shows the formation of supramolecular 3D network in **H_2L^1-O** through the intermolecular C−H···O, efficient π-π interaction (Figure 6c).

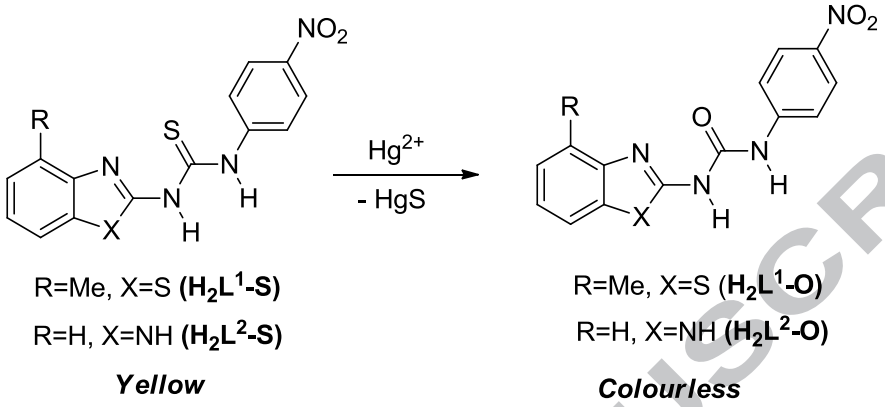

Scheme 2. Hg^{2+}-selective signalling mechanism of thiourea based chemodosimeter **H_2L^1-S** and **H_2L^2-S**

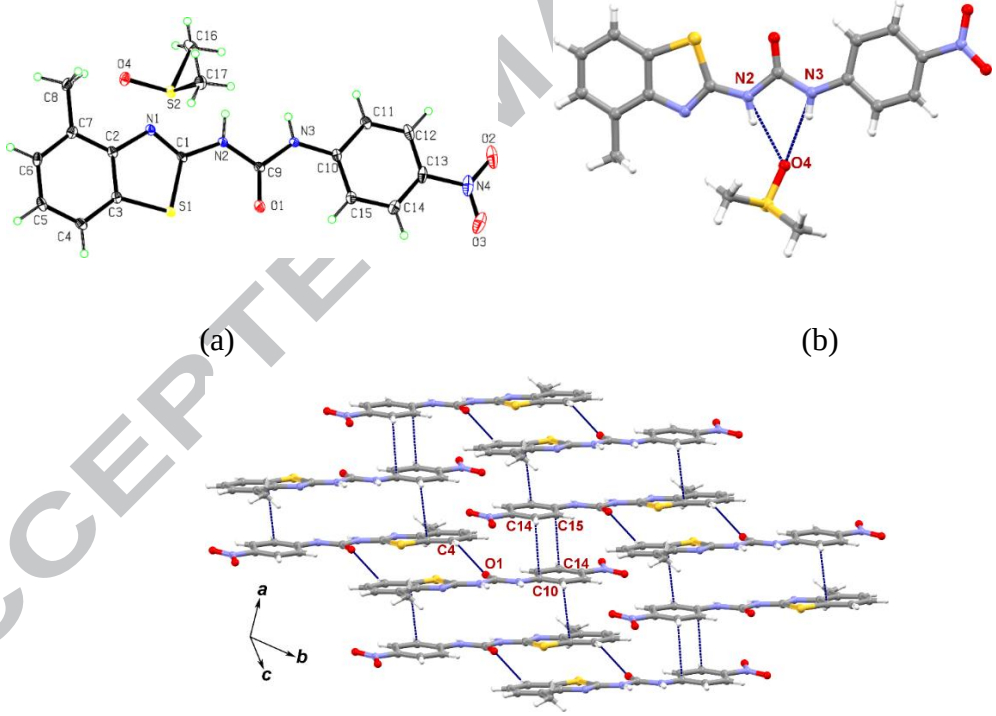

Figure 6. (a) Crystal structure of the compound **H_2L^1-O** with 30 % ellipsoid probability. (b) View of the intermolecular hydrogen bonding interaction in the compound with solvent DMSO molecule. (c) View of the supramolecular 3D network in compound **H_2L^1-O.**

3.3.3 Theoretical Study

To gain insight into the electronic transitions and relation between structural and molecular spectral changes of **H_2L^1-S** and **H_2L^2-S** upon Hg^{2+} addition, the geometry optimization and time-dependent DFT (TD-DFT) calculations were carried out in DMSO. The transitions in the UV−visible region between 280 and 540 nm are assigned to various electronic transitions. Selected calculated molecular orbitals (MOs) and geometry optimized structures of **H_2L^1-S**, **H_2L^2-S, H_2L^1-O** and **H_2L^2-O** are shown in Figure 7. The final products, **H_2L^1-O** (E = −49508.78 eV) and **H_2L^2-O** (E = −39111.45 eV) are more stable than **H_2L^1-S** (E = −49505.24eV) and **H_2L^2-S** (E = −39106.83 eV) and the stability is gained as 3.5 eV and 4.6 eV free energy is released, respectively. In Table S1 (see SI), the computed vertical excitation energies and composition of the related transitions assigned to the experimental UV−vis spectra and theoretical UV−vis spectra (Figure S16) are displayed. The TD-DFT calculations for **H_2L^1-S** indicate that the experimental transition band at ~370 nm arises from a strong transition characterized as HOMO→ LUMO (f = 0.12, λ_{max} = 391.84 nm). In contrast, for **H_2L^1-O,** the band centered at 340 nm is due to the HOMO−2 →LUMO (f = 0.29, λ_{max} = 334 nm) transition. In **H_2L^2-S**, experimental transition band at 375 nm is due to the transitions from HOMO−1 →LUMO and HOMO−2 → LUMO (f = 0.10, λ_{max}= 376.48 nm) whereas, in **H_2L^2-O** the band at 270 nm is due to the HOMO →LUMO+2 (f = 0.45, λ_{max} = 263.04 nm) transition.

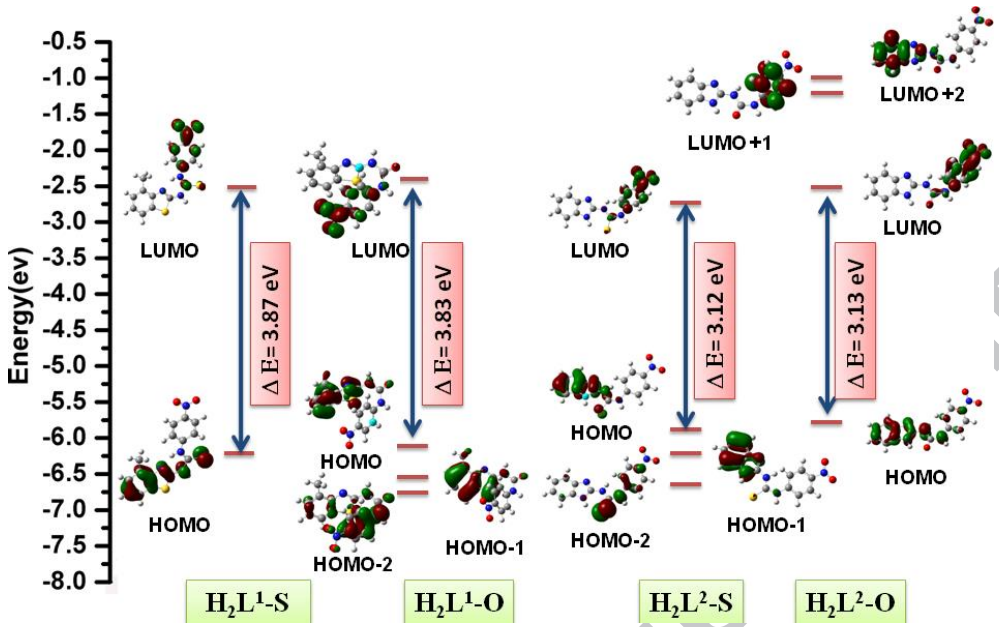

Figure 7. View of the frontier molecular orbitals (MOs) of **H_2L^1-S**, **H_2L^2-S, H_2L^1-O** and **H_2L^2-O** [isovalue = 0.03].

3.4 *Acetate (AcO^-) Detection in Fluorescence Spectroscopy*

3.4.1 Fluorescence spectral changes of probes in the presence of AcO^-

The aptitude of **H_2L^1-S** and **H_2L^2-S** to serve as probes for different anions (100.0 equiv.) was tested in fluorescence spectroscopy in DMSO at room temperature. In the fluorescence channel, probes **H_2L^1-S** and **H_2L^2-S** display a very weak fluorescence band at 465 (Φ = 0.008) and 460 nm (Φ = 0.012), respectively (λ_{ex} = 412 and 405 nm) in DMSO at 25 °C. Both the probes, **H_2L^1-S** and **H_2L^2-S** show maximum fluorescence enhancement only in the presence of AcO^- at 493 nm (Φ = 0.095 and 0.083 respectively) and greenish blue fluorescence (Figure 8a and 8b inset) while other anions such as F^-, Cl^-, Br^-, I^-, $H_2PO_4^-$, HSO_4^-, PPi, CN^-, N_3^-, $S_2O_3^{2-}$, SO_4^{2-}could only give negligible fluorescence increase (Figure 8a, b). During fluorescence titration in DMSO, ~10-fold (Figure 9a) fluorescence intensity enhancement is observed for **H_2L^1-S** in the presence of 100 equiv. of AcO^- (for **H_2L^2-S,** ~4-fold; Figure 9b). The nonlinear curve fitting analysis from the fluorescence titration data of **H_2L^1-S** and **H_2L^2-S** with AcO^- shows good fit with the 1:1 model (R = 0.9936 and 0.98775

respectively). (Figure 10a, 10b). Moreover, the Job plot analysis also showed the inflection point at 0.5, signifying a 1:1 stoichiometry between probe **H_2L^1-S** and **H_2L^2-S** toward AcO^-. (Figure S17, S18). Under well-established sensing conditions, the detection limit of **H_2L^1-S** and **H_2L^2-S** was calculated to be as low as 0.47 μM and 0.15 μM respectively (Figure S19, S20) from fluorescence titration data in DMSO. This specifies that these probes can be used to detect very low concentration of AcO^-.

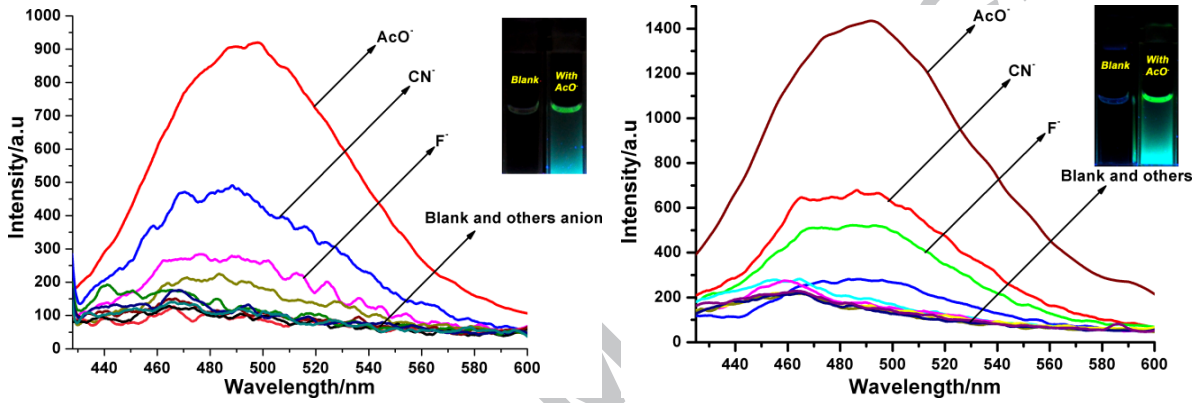

Figure 8. (a) Fluorescence spectra of (a) **H_2L^1-S** (50 μM, λ_{ex} = 412 nm, λ_{em} = 493 nm) (b) **H_2L^2-S** (50 μM, λ_{ex} = 405 nm, λ_{em} = 493 nm) with various anions, (100 equiv). (*Inset*) Naked eye fluorescence colour change under UV light.

The fluorescence lifetime (τ) of **H_2L^1-S** (0.04 ns) and **H_2L^2-S (**0.33 ns)**,** measured in DMSO, were increased to 2.89 and 2.79 ns respectively in the presence of 100 equiv. of AcO^- (Figure 11 a, b). Also, a time-dependent fluorescence response studies were carried out for both the probes **H_2L^1-S** and **H_2L^2-S** with 100 equiv. of AcO^- over 20 mins. As shown in Figure 12 (a and b), a steady fluorescence intensity enhancement is observed during the first 1.5 min before it reaches to saturation.

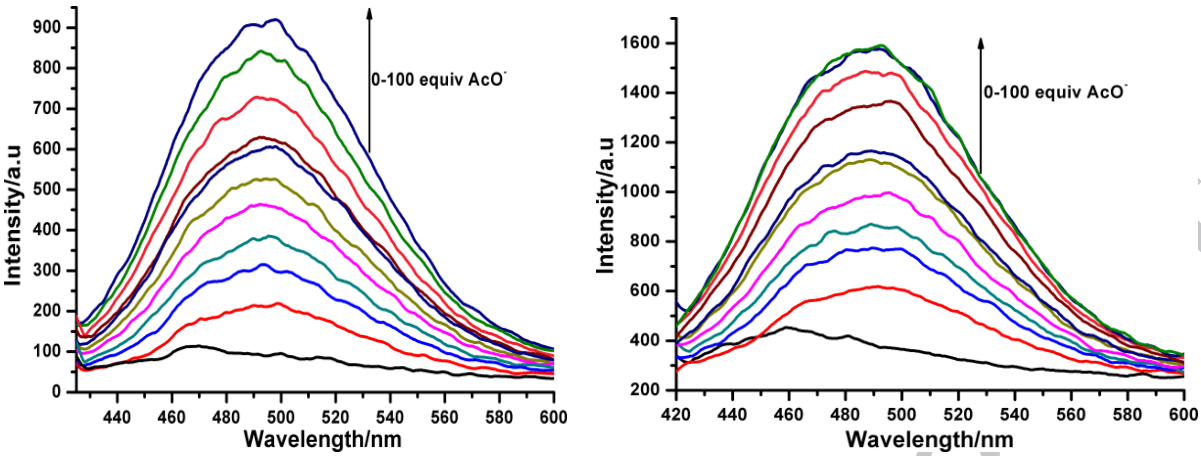

Figure 9. Fluorescence titration of (a) **H_2L^1-S** (50 μM) (b) **H_2L^2-S** (50 μM) in DMSO with increasing amount of AcO^- solution (0-100 equiv.).

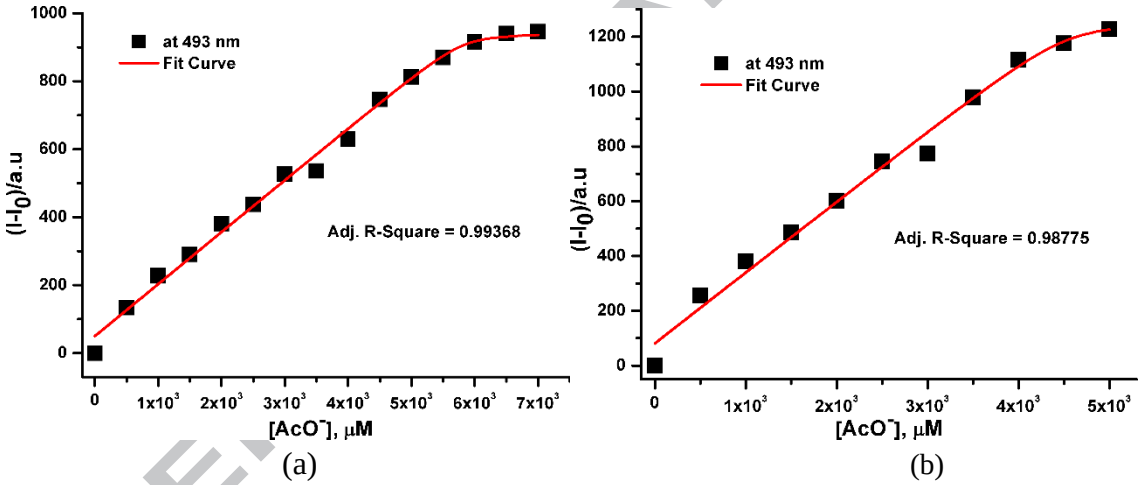

Figure 10. Non-Linear curve fitting for the 1:1 model from the PL titration of (a) H_2L^1-S (b) H_2L^2-S with AcO^- Binding (λem = 493 nm).

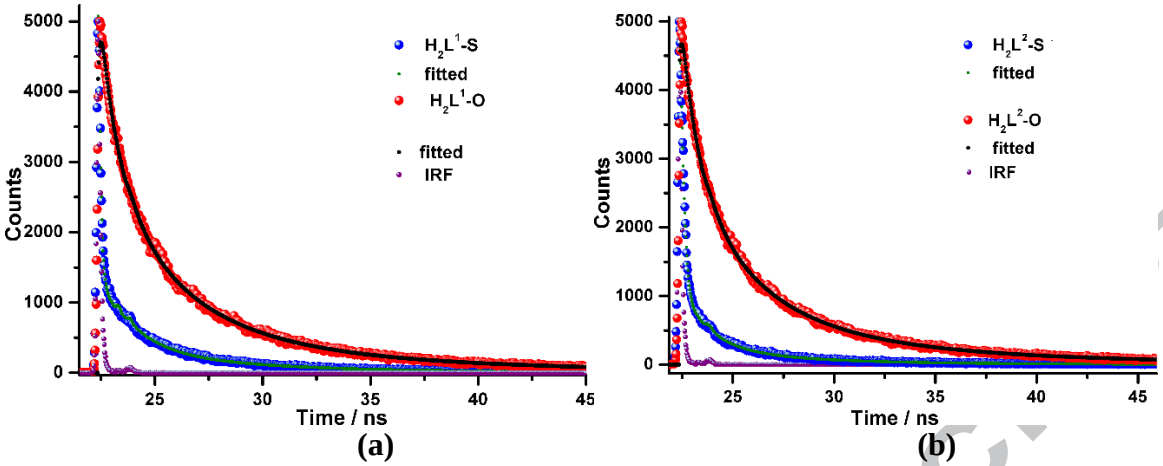

Figure 11. Time resolved fluorescence spectra of (a) H_2L^1-S (50 μM) (b) H_2L^2-S (50 μM) before and after addition of AcO^- in DMSO.

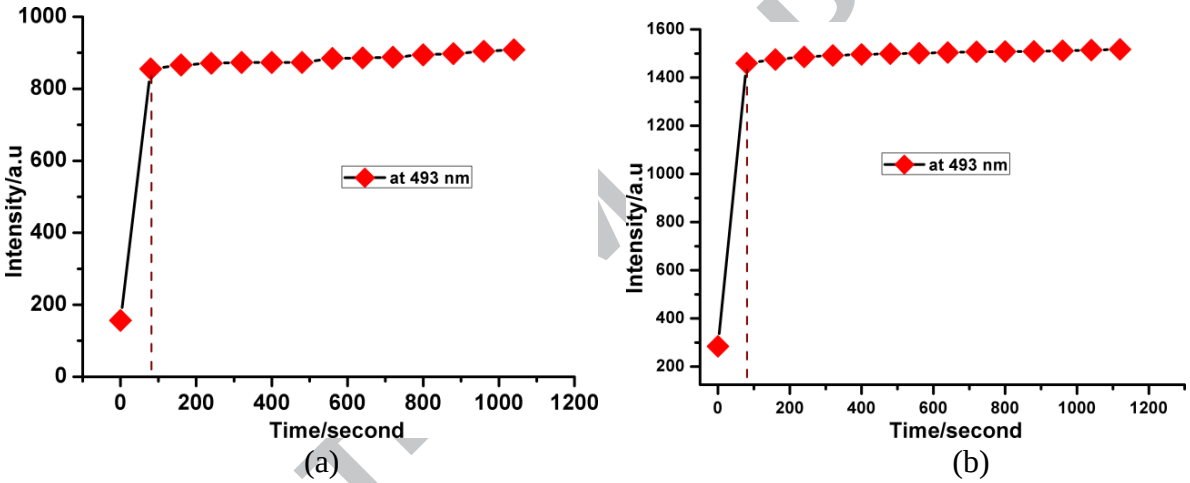

Figure 12. Time course of the fluorescence response of (a) **H_2L^1-S** (b) **H_2L^2-S** with 100 equiv. of AcO^- in DMSO at 493 nm.

The PL response of **H_2L^1-S** and **H_2L^2-S** toward AcO^- (100 equiv) the presence of other competitive anions and mercury (500 equiv.) were measured to examine the possible interference. The tested anions and Hg^{2+} did not interfere in AcO^- detection in fluorescence spectroscopy channel. (Figure S21, S22)

3.4.2 Plausible mechanism and ESI–MS analysis:

The proposed mechanism for the AcO^- detection by the probes **H_2L^1-S** and **H_2L^2-S** is described in Scheme 3. As reported earlier [46], here we assumed that the deprotonation of **H_2L^1-S** and **H_2L^2-S** by the AcO^- ion increased the electron density in the *p*-nitrobenzene

moiety. Probe **H_2L^1-S** and **H_2L^2-S** shows very weak fluorescence band due to the photo-induced electron transfer (PET) from benzothiazole/benzimidazole to *p*-nitrobenzene moiety. While, due to the formation of deprotonated species, **$[L^1\text{-}S]^{2-}$** and **$[HL^2\text{-}S]^-$** after to the interaction of AcO^- with **H_2L^1-S** and **H_2L^2-S,** the electron density in *p*-nitrobenzene moiety is slightly increased and photo induced electron transfer process (PET) is inhibited, consequently, the probes emit strongly from the benzothiazole/benzimidazole based locally excited (LE) state. All the fluorescence AcO^- sensing data were recorded in pure DMSO solution because in the aqueous solution the water molecule converts the deprotonated species to probe **H_2L^1-S** and **H_2L^2-S** and reinstates the PET from benzothiazole/benzimidazole moiety to p-nitrobenzene (Figure S23, S24). The formation of **$[L^1\text{-}S]^{2-}$** and **$[HL^2\text{-}S]^-$** was confirmed by ESI-MS analysis as the peak at m/z 397.07 (calcd. = 397.05) (Figure S25) and 312.08 (calcd. = 312.06) (Figure S26) corresponding to $[C_{15}H_{12}N_4O_2S_2 - 2H + CH_3OH + Na^+]^-$ and $[C_{14}H_{11}N_5O_2S - H]^-$ was clearly observed.

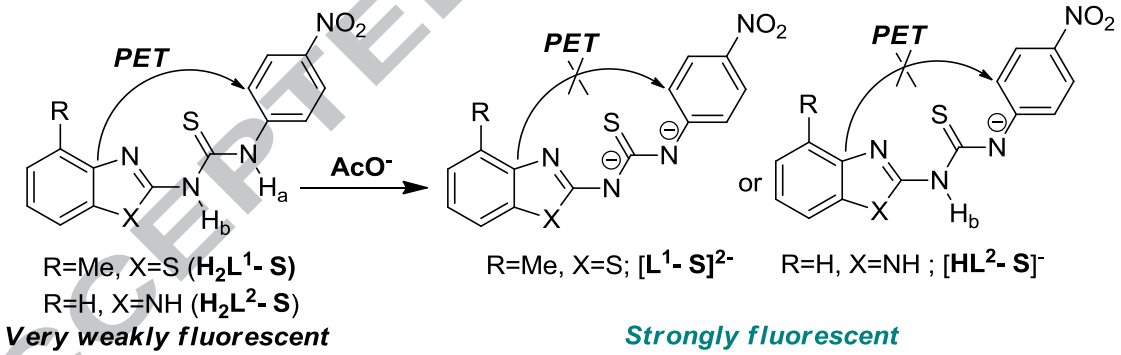

Scheme 3. Plausible mechanism for fluorometric acetate ion detection.

3.5 Live Cell Imaging and Cytotoxicity Study:

The biological usefulness of probe **H_2L^1-S** was assessed by screening its cytotoxicity in HEK293T cell for 24 h. A concentration dependent cytotoxicity of probe **H_2L^1-S** was observed (Figure S27). More than 70% cell viability was observed at 50 μM (working concentration) and 58% viability at 100 μM (Maximum concentration) of probe **H_2L^1-S** after

24 h of treatment. This data implies the less toxicity of probe **H_2L^1-S** over a broad concentration range.

On the basis of the cytotoxicity results, we investigated the ability of **H_2L^1-S** to detect AcO^- in biological systems by staining of living cells. As shown in Figure 13, incubation of HEK293T cells with **H_2L^1-S** (50 μM) for 30 min failed to exhibit any fluorescence in the green channel. Interestingly, when the probe **H_2L^1-S** loaded cells were subsequently exposed to 50μM AcO^-, a bluish green fluorescence was displayed. These results indicate that probe **H_2L^1-S** has the potential to detect AcO^- levels in living cells.

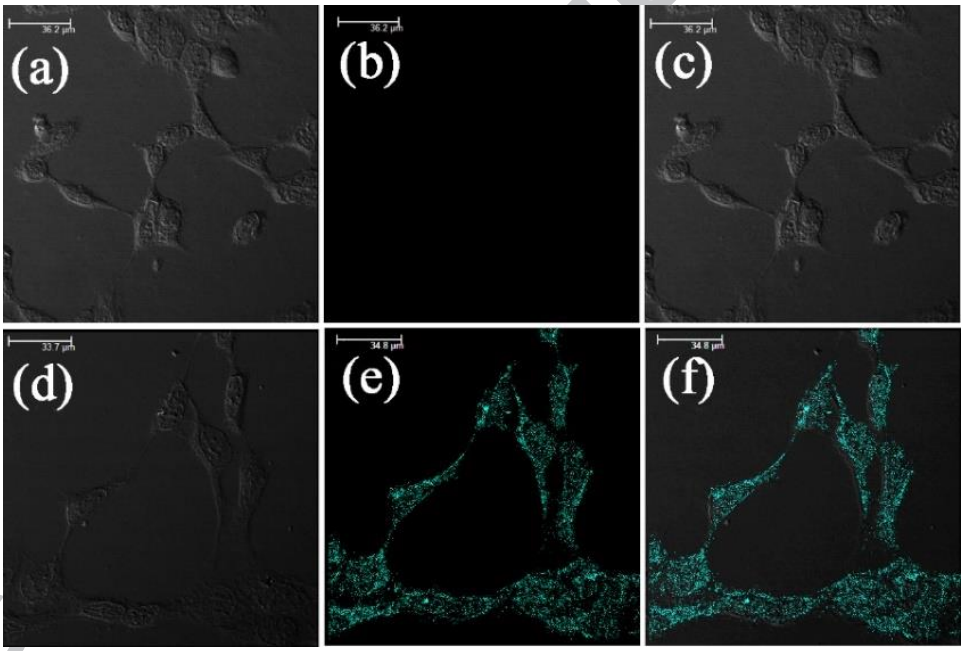

Figure 13. Bright field, fluorescence, and overlay images of (a-c) HEK293T cells treated with only **H_2L^1-S** (50 μM), (d−f) HEK293T cells treated with **H_2L^1-S** (50μM) and AcO^- (100 equiv).

4. Conclusions

We have developed two new thio-urea based bifunctional probes, **H_2L^1-S** and **H_2L^2-S** and characterized them by several spectroscopies as well as single crystal X-ray diffraction. We have shown that both the probes selectively detected Hg^{2+} ion through the colour change from yellow to colourless associated with a notable blue shift through the formation of Hg^{2+}

ion-promoted desulfurized product. This transformation was confirmed by ESI–MS, and also supported by TDDFT calculation. Most interestingly, the desulfurized product **H_2L^1-O** was separated and characterized by single crystal X-ray diffraction. The probes can quantify Hg^{2+} at the micromolar level even in the presence of other cations which is demonstrated by interference study. In the fluorescence channel, the **H_2L^1-S** and **H_2L^2-S** acted as turn-on fluorescent probe for AcO^- ion in DMSO solution through the inhibition of PET. The calculated detection limits suggested that the probes can detect AcO^- in sub-micromolar level. The fluorescence time course indicated that the deprotonation reaction of AcO^- with the probes was completed within ~1.5 min. The cytotoxicity and live cell imaging study using HEK293T cells with the probe revealed that the probe has low cytotoxicity, good cell membrane permeability and is capable for exogenous AcO^- imaging.

Acknowledgements

We thank DST SERB (SB/FT/CS/115/2012) for the financial assistance and Sophisticated Analytical and Instrumentation Facility (SAIF), North Eastern Hill University for NMR and MS data. S.P., B.S and S.K.S. thank North Eastern Hill University, CSIR (SRF) and UGC respectively for their research fellowship. Mr. D. Koner, Dept. of Zoology, NEHU is gratefully acknowledged for his help in cell imaging study.

Appendix A. Supplementary data

Supplementary data associated with this article can be found, in the online version, at http://dx.doi.org/.

References

1. K. Chen, Q. Shu, M. Schmittel, Design Strategies for Lab-on-a molecule Probes and Orthogonal Sensing, Chem. Soc. Rev. 44 (2015) 136−160.
2. S. K. Sheet, B. Sen, R. Thounaojam, K. Aguan, S. Khatua, Highly Selective Light-up Al^{3+} Sensing by a Coumarin Based Schiff Base Probe: Subsequent Phosphate Sensing DNA Binding and Live Cell Imaging. J. Photochem. Photobiol. A: Chem 332, (2017), 101−111.
3. R. Singh, G. Das, Fluorogenic detection of Hg^{2+} and Ag^{+} ions via two mechanistically discrete signal genres: A paradigm of differentially responsive metal ion sensing, Sensors and Actuators B. 258 (2018) 478–483.
4. L. Yuan, W. Lin, Y. Xie, B. Chen, S. Zhu, Single Fluorescent Probe Responds to H_2O_2, NO, and H_2O_2/NO with Three Different Sets of Fluorescence Signals, J. Am. Chem. Soc. 134 (2012) 1305−1315
5. P.G. Sutariya, N. R. Modi, A. Pandya, B. K. Joshi, K. V. Joshi, S. K. Menon, An ICT based ‘‘*turn on/off*’’ quinoline armed calix [4] arene fluoroionophore: its sensing efficiency towards fluoride from waste water and Zn^{2+} from blood serum, Analyst, 137 (2012) 5491–5494.
6. Y. Peng, Y.M. Dong, M. Dong, Y.W. Wang, A Selective, Sensitive, Colorimetric, and Fluorescence Probe for Relay Recognition of Fluoride and Cu(II) Ions with “Off−On−Off” Switching in Ethanol−Water Solution, J. Org. Chem. 77 (2012) 9072–9080.
7. L. N. Neupane, J.-Y. Park, J. H. Park, K.-H. Lee, Turn-On Fluorescent Chemosensor Based on an Amino Acid for Pb(II) and Hg(II) Ions in Aqueous Solutions and Role of Tryptophan for Sensing. Org. Lett. 15 (2013) 254−257.

8. S. K. Sheet, B. Sen, R. Thounaojam, K. Aguan, S. Khatua, Ruthenium (II) Complex-Based Luminescent Bifunctional Probe for Ag^{+} and Phosphate Ions: Ag^{+}–Assisted Detection and Imaging of rRNA, Inorg. Chem. 56 (2017) 1249−1263.
9. S. Sakunkaewkasem, A. Petdum, W. Panchan, J. Sirirak, A. Charoenpanich, T. Sooksimuang, N. Wanichacheva, Dual-Analyte Fluorescent Sensor Based on [5]Helicene Derivative with Super Large Stokes Shift for the Selective Determinations of Cu^{2+} or Zn^{2+} in Buffer Solutions and Its Application in a Living Cell, ACS Sens. 3 (2018) 1016−1023.
10. M, Schmittel, H.W. Lin, Quadruple-Channel Sensing: A Molecular Sensor with a Single Type of Receptor Site for Selective and Quantitative Multi-Ion Analysis, Angew. Chem. Int. Ed. 46 (2007) 893 –896.
11. K. Chen, M. Schmittel, An iridium (III)-based lab-on-a-molecule for cysteine/ homocysteine and tryptophan using triple-channel interrogation, Analyst. 138 (2013) 6742−6745.
12. M. Wang, F. Yan, Y, Zou, L. Chen, N. Yang, X. Zhou, Recognition of Cu^{2+} and Hg^{2+} in physiological conditions by a new rhodamine based dual channel fluorescent probe, Sens. Actuators, B. 192 (2014) 512– 521.
13. Y. Li, J. Wu, X. Jin, J. Wang, S. Han, W. Wu, J. Xu, W. Liu, X. Yao, Y. Tang, A bimodal multianalyte simple molecule chemosensor for Mg^{2+}, Zn^{2+}, and Co^{2+}, Dalton Trans., 43 (2014) 1881–1887.
14. S.M. Hwang, C. Kim, Fluorescent detection of Zn^{2+} and Cu^{2+} by a phenanthrene-based multifunctional chemosensor that acts as a basic pH indicator, Inorg. Chim. Acta, 482 (2018) 375–383.

15. B. X. Shen, Y. Qian, Building Rhodamine-BODIPY fluorescent platform using Click reaction: Naked-eye visible and multi-channel chemodosimeter for detection of Fe^{3+} and Hg^{2+}, Sens. Actuators, B. 260 (2018) 666–675.

16. A. K. Mahapatra, R. Maji, K. Maiti, S. S. Adhikari, C. D. Mukhopadhyay, D. Mandal, Ratiometric sensing of fluoride and acetate anions based on a BODIPY-azaindole platform and its application to living cell imaging, Analyst, 139 (2014) 309.

17. S. Samanta, P. Dey, A. Ramesh, G. Das, A Solo Fluorogenic Probe for the Real-Time Sensing of SO_3^{2-} and SO_4^{2-}/HSO_4^- in Aqueous Medium and Live Cells by Distinct Turn-On Emission Signals, Chem. Commun., 52 (2016) 10381.

18. S. K. Patra, S. K. Sheet, B. Sen, K. Aguan, D. R. Roy, S. Khatua, Highly Sensitive Bifunctional Probe for Colorimetric Cyanide and Fluorometric H_2S Detection and Bioimaging: Spontaneous Resolution, Aggregation, and Multicolor Fluorescence of Bisulfide Adduct. J. Org. Chem. 82 (2017) 10234−10246.

19. T. Ábalos, D. Jiménez, M. Moragues, S. Royo, R. Martıń ez-Mañ ez, F. Sancenoń, J. Soto, A. M. Costero, M. Parra, S. Gil, Multi-channel receptors based on thiopyrylium functionalised with macrocyclic receptors for the recognition of transition metal cations and anions, Dalton Trans. 39 (2010) 3449−3459.

20. J. Y. Yun, J. B. Chae, M. Kim, M. H. Lim, C. Kim, A multiple target chemosensor for the sequential fluorescence detection of Zn^{2+} and S^{2-} and the colorimetric detection of $Fe^{3+/2+}$ in aqueous media and living cells, Photochem. Photobiol. Sci., (2019) DOI. 10.1039/C8PP00408K.

21. E. M. Nolan, S. J. Lippard, Tools and Tactics for the Optical Detection of Mercuric Ion, Chem. Rev. 108 (2008) 3443–3480.

22. H Ozay, R Kagit, M Yildirim, S Yeşilot, O Ozay, Novel hexapodal triazole linked to a cyclophosphazene core rhodamine-based chemosensor for selective determination of Hg^{2+} ions, J Fluoresc 24 (2014) 1593–1601.
23. P. Samanta, A. V. Desai, S. Sharma, P. Chandra, S.K. Ghosh, Selective Recognition of Hg(II) ion in Water by a Functionalized Metal-Organic Framework (MOF) Based Chemodosimeter, Inorg. Chem. 57 (2018) 2360-2364.
24. S. Ando, K. Koide, Development and Applications of Fluorogenic Probes for Mercury (II) Based on Vinyl Ether Oxymercuration, J. Am. Chem. Soc. 133 (2011) 2556–2566.
25. G. Chen, Z. Guo, G. Zeng, L. Tang, Fluorescent and colorimetric sensors for environmental mercury detection, Analyst. 140 (2015) 5400–5443.
26. S. Manna, P. Karmakar, K. Maiti, S. S. Ali, D. Mandal, A. K. Mahapatra, A reactive primary fluorescence switch-on sensor for Hg^{2+} and the generated fluorophore as secondary recognition receptor toward Cu^{2+} in aqueous acetonitrile solution, J. Photochem. Photobiol. A: Chem, 343 (2017) 7–16.
27. S. Khatua, M. Schmittel, A Single Molecular Light-up Sensor for Quantification of Hg^{2+} and Ag^{+} in Aqueous Medium: High Selectivity toward Hg^{2+} over Ag^{+} in a Mixture, Org. Lett. 15 (2013) 4422–4425.
28. K.G. Harshaa, E. Appalanaidu, N. R. Chereddy, T.R. Baggi, V. J. Rao, Pyrene tethered imidazole derivative for the qualitative and quantitative detection of mercury present in various matrices, Sens. Actuators, B 256 (2018) 528–534.
29. S. O. Tümay, A. Uslu, H. A. Alidağı, H. H. Kazan, C. Bayraktar, T. Yolaçan, M. Durmuş, S. Yeşilot, A systematic series of fluorescence chemosensors with multiple binding sites for Hg(II) based on pyrenyl-functionalized cyclotriphosphazenes and their application in live cell imaging. New J. Chem., 42 (2018) 14219-14228

30. K. Chen, S. She, J. Zhang, A. Bayaguud, Y. Wei, Label-free colorimetric detection of mercury via Hg^{2+} ions-accelerated structural transformation of nanoscale metal-oxo clusters. Sci. Rep. 5 (2015)16316.
31. S. Zhang, D. Zhang, X. Zhang, D. Shang, Z. Xue, D. Shan, X. Lu, Ultratrace Naked-Eye Colorimetric Detection of Hg^{2+} in Wastewater and Serum Utilizing Mercury-Stimulated Peroxidase Mimetic Activity of Reduced Graphene Oxide-PEI-Pd Nanohybrids, Anal. Chem. 89 (2017) 3538−3544.
32. S. Vallejos, J. A. Reglero, F. C. García, J. M. García, Direct visual detection and quantification of mercury in fresh fish meat using facilely prepared polymeric sensory labels, J. Mater. Chem. A. 5 (2017) 13710–13716.
33. C. Suksai, T, Tuntulani, Chromogenic anion sensors, Chem. Soc. Rev., 32 (2003) 192-202.
34. P. Bose, B. N. Ahamed, P. Ghosh, Functionalized guanidinium chloride based colourimetric sensors for fluoride and acetate: single crystal X-ray structural evidence of -NH deprotonation and complexation, Org. Biomol. Chem., 9 (2011) 1972–1979
35. S. B. Maity, P. K. Bharadwaj, A Chemosensor Built with Rhodamine Derivatives Appended to an Aromatic Platform via 1,2,3-Triazoles: Dual Detection of Aluminum(III) and Fluoride/Acetate Ions, Inorg. Chem. 52 (2013) 1161−1163.
36. A. Singh, S. Tom, D. R. Trivedi, Aminophenol based colorimetric chemosensor for naked-eye detection of biologically important fluoride and acetate ions in organo-aqueous medium: Effective and simple anion sensors, J. Photochem. Photobiol. A: Chem, 353 (2018) 507–520
37. W. Huang, H. Lin, H. Lin, Fluorescent acetate-sensing in aqueous solution, Sens. Actuators, B 2011 (153) 404-408.

38. V. K. Gupta, A. K. Singh, N, Gupta, Colorimetric sensor for cyanide and acetate ion using novel biologically active hydrazones 2014 (204) 125-135.

39. S. Goswami, A. K. Das, D. Sen, K. Aich, H-K. Fun, C. K. Quah, A simple naphthalene-based colorimetric sensor selective for acetate, Tetrahedron Letters, 53 (2012) 4819–4823

40. A. Ghosh, A. Sengupta, A. Chattopadhyay, D. Das, A Single Probe for Sensing Both Acetate and Aluminium (III): Visible Region Detection, Red Fluorescence and Human Breast Cancer Cell Imaging, RSC Advances 5(2015) 24194-24199.

41. P. Singh, H. Singh, G. Bhargava, S. Kumar, Triple-signalling mechanisms-based three-in-one multi-channel chemosensor for discriminating Cu^{2+}, acetate and ion pair mimicking AND, NOR, INH and IMP logic functions, Journal of Materials Chemistry C, 3 (2015) 5524-5532

42. Q. Lin, X. Liu, T.-B. Wei, Y.-M. Zhang, TICT-ICT state change mechanism based acetate fluorescent sensor act as an "off-On-Off" switch and logic gate, Sens. Actuators, B: Chemical 190(2014) 459-463.

43. A. P. De. Silva, H. Q. N. Gunaratne, T. Gunnlaugsson, A. J. M. Huxley, C. P. McCoy, J. T. Rademacher, T. E. Rice, Signaling Recognition Events with Fluorescent Sensors and Switches, Chem. Rev. 97 (1997) 1515-1566.

44. S. T. Manjare, J. Kim, Y. Lee, D. G. Churchill, Facile *meso*- BODIPY Annulation and Selective Sensing of Hypochlorite in Water, Org. Lett. 16 (2014) 520−523.

45. T. Yudhistira, S. V. Mulay, K. J. Lee, Y. Kim, H-S. Park, D. G. Churchill, Thiomaleimide Functionalization for Selective Biological Fluorescence Detection of Peroxynitrite as Tested in HeLa and RAW 264.7 Cells, Chem. Asian J. 12 (2017) 1927 – 1934

46. A.-F. Li, J.-H. Wang, F. Wang, Y.-B. Jiang, Anion complexation and sensing using modified urea and thiourea-based receptors, Chem. Soc. Rev. 39 (2010) 3729–3745.

47. K. Tsukamoto, Y. Shinohara, S. Iwasaki, H. Maeda, A coumarin-based fluorescent probe for Hg^{2+} and Ag^{+} with an N′-acetylthioureido group as a fluorescence switch, Chem. Commun., 47 (2011) 5073–5075.

48. S. Khatua, D. Samanta, J. W. Bats, M. Schmittel, Rapid and Highly Sensitive Dual-Channel Detection of Cyanide by Bis-heteroleptic Ruthenium(II) Complexes, Inorg. Chem., 51 (2012) 7075–7086.

49. B. Sen, S. K. Sheet, R. Thounaojam, R. Jamatia, A. K. Pal, K. Aguan, S. Khatua, A coumarin based Schiff base probe for selective fluorescence detection of Al^{3+} and its application in live cell imaging, Spectrochim. Acta, Part A, 173 (2017) 537−543.

50. S. K. Sheet, B. Sen, S. K. Patra, M. Rabha, K. Aguan, Snehadrinarayan Khatua, Aggregation-Induced Emission-Active Ruthenium(II) Complex of 4,7-Dichloro Phenanthroline for Selective Luminescent Detection and Ribosomal RNA Imaging, ACS Appl. Mater. Interfaces, 10 (2018) 14356–14366

51. S. K. Sheet, B. Sen, K. Aguan, S. Khatua, A cationic organoiridium(III) complex-based AIEgen for selective light-up detection of rRNA and nucleolar staining, Dalton Trans.,47 (2018) 11477-11490.

52. S. K. Sheet, B. Sen, S. Khatua, Organoiridium(III) Complexes as Luminescence Color Switching Probes for Selective Detection of Nerve Agent Simulant in Solution and Vapor Phase. Inorg. Chem.58 (2019) 3635–3645.

53. C. Lee, W. Yang, R.G. Parr, Development of the Colic-Salvetti correlation-energy formula into a functional of the electron density, Phys. Rev. B 37 (1988) 785– 789.

54. A.D. Becke, Density-functional thermochemistry. III. The role of exact exchange, J. Chem. Phys. 98 (1993) 5648–5652.

55. CrysAlisPro Software System, 1.171.36.28; Agilent Technologies UK Ltd.: Oxford, UK, (2013).

56. Sheldrick, G. M. SHELXS-97: Program for Crystal Structure Determination. Acta Crystallogr. A46 (1990) 467–473.

57. G. M. Sheldrick, A Short History of SHELX. Acta Cryst., A64 (2008) 112-122.

58. SAINT Plus, version 7.03; Bruker AXS, Inc.: Madison, WI, 2004.

59. SADABS, Area Detector Absorption Correction Program; Bruker Analytical X-ray: Madison WI, 1997.

60. Altomare, A.; Cascarano, G.; Giacovazzo, C.; Guagliardi, A.; Burla, M.C.; Polidori, G.; Camalli, G. SIR92 – A Program for Automatic Solution of Crystal Structures by Direct Methods. J. Appl. Crystallogr., 27 (1994) 435–435.

61. A. L. Spek, PLATON: A Multipurpose Crystallographic Tool, Utrecht University, The Netherlands, 1998.

62. G. Zhang, D. Zhang, S. Yin, X. Yang, Z. Shuai, D. Zhu, 1,3-Dithiole-2-thione derivatives featuring an anthracene unit: new selective chemodosimeters for Hg(II) ion, Chem. Commun., (2005) 2161–2163.

Graphical abstract

Single Molecular Dual Analyte Thio-Urea based Probes for Colorimetric Hg^{2+} and Fluorometric AcO^{-} Detection and Its'Application in Bioimaging

Sumit Kumar Patra,[a] Bhaskar Sen,[a] Sanjoy Kumar Sheet,[a] Bodhisattwa Banerjee,[b] Nirmalendu Saha,[b] Snehadrinarayan Khatua* [a]

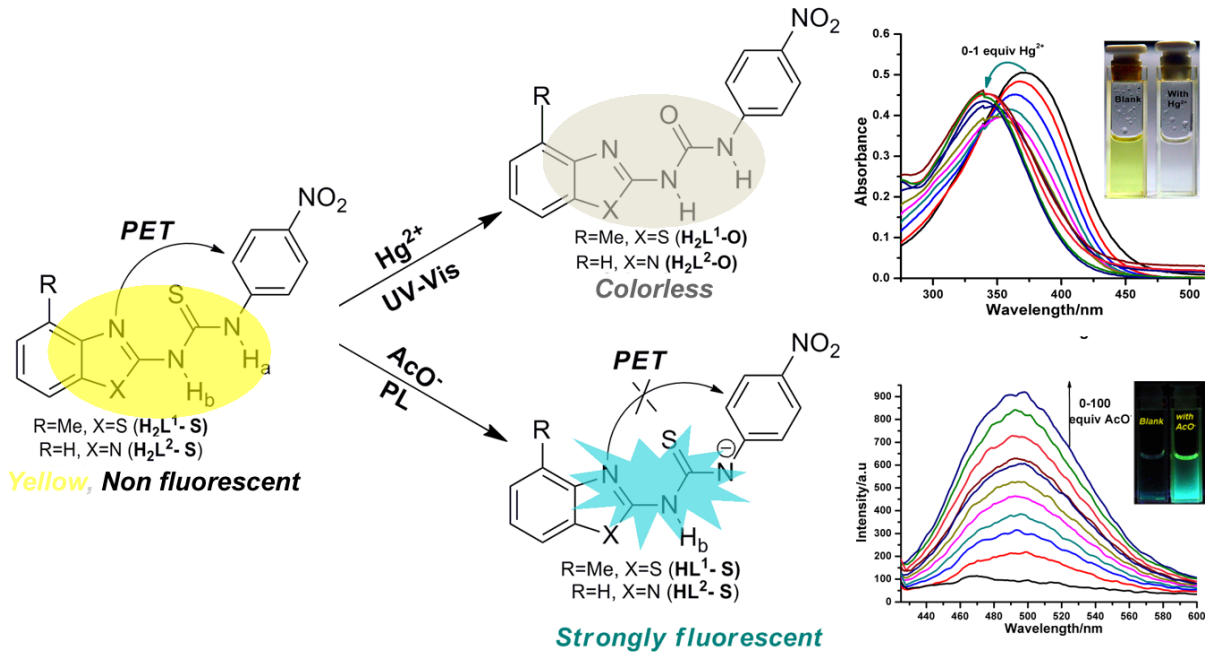

Thio urea based bifunctional probes for highly selective colorimetric Hg^{2+} and fluorescence "light-up" AcO^{-} detection are presented here. Live cell imaging by the probe and AcO^{-} is also discussed herein.

Highlights

- Thio-urea based bifunctional probe for colorimetric Hg^{2+} and fluorometric AcO^- ion detection.
- ESI-MS and single crystal structural support for Hg^{2+} ion-promoted desulfurization.
- Fluorescence light-up acetate ion detection through inhibition of PET.
- Detection and quantification of AcO^- at its low concentration (detection limit = 0.47μM and 0.15 μM) and its application in cell imaging.